analytical chemistry

Article

Cite This: Anal. Chem. XXXX, XXX, XXX−XXX

pubs.acs.org/ac

Fabrication of Magnetic Conjugation Clusters via Intermolecular Assembling for Ultrasensitive Surface Plasmon Resonance (SPR) Detection in a Wide Range of Concentrations

Zhichao Lou,*[,†,‡] He Han,[†] Ming Zhou,[†] Jinfeng Wan,[†] Qian Sun,[†] Xiaoyan Zhou,[†] and Ning Gu*[,‡]

[†]College of Materials Science and Engineering, Nanjing Forestry University, Nanjing 210037, China

[‡]State Key Laboratory of Bioelectronics, Jiangsu Key Laboratory for Biomaterials and Devices, School of Biological Science and Medical Engineering, Southeast University, Nanjing 210096, China

Supporting Information

ABSTRACT: Herein, a novel sandwich surface plasmon resonance (SPR) detection assay, which utilizes prion disease-associated isoform (PrP^{Sc}) conjugating magnetic nanoparticle clusters (nanoparticle−organic clusters, NOCs) as signal amplification reagents, is constructed for the ultrasensitive detection of PrP^{Sc}. Due to the highly specific affinity of aptamer−Fe_3O_4 nanoparticles (AMNPs) toward PrP^{Sc} and the intermolecular assembly behaviors among PrP^{Sc}, PrP^{Sc} conjugating magnetic nanoparticle clusters were obtained after the incubation of AMNPs and PrP^{Sc} and the subsequent concentration processes in an external magnetic field. The conjugation clusters were further injected into the SPR cuvette and captured by the gold sensing film via the Au−S bonding interaction, inducing intense SPR responses. Meanwhile, a traditional sandwich SPR detection format using a gold/PrPSc/AMNPs amplification mode was conducted for the detection of PrP^{Sc} as comparison. The results reveal that the synthesized NOCs permitted a 215-fold increase of the SPR signal, while the sandwich format permitted only a 65-fold increase. Moreover, a lower detection limit (1×10^{-4} ng/mL) and a wider quantitation range (1×10^{-4}−1×10^{5} ng/mL) were demonstrated. The formation of the conjugation clusters and the capture of these clusters were confirmed by high-resolution AFM imaging and molecular simulations. This conjugation-cluster-induced signal amplification strategy has great potential for the detection of small analytes with similar structural characteristics in trace level concentrations with high selectivity and sensitivity by altering the corresponding aptamer labeled to magnetic particles.

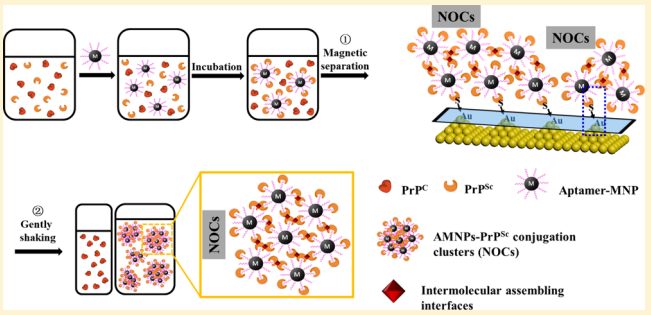

Prion protein (PrP) is a cell surface glycoprotein, which cycles between the cell surface and endocytic compartment.[1,2] Two isoforms of PrP have been designated PrP^{C} and PrP^{Sc}; they have the same amino acid sequence but are different in conformation. The conversion of PrP^{C} to PrP^{Sc} is the mechanism of transmission of fatal, neurodegenerative transmissible spongiform encephalopathies (TSE).[3] PrP^{Sc} is an early biomarker for the diagnostics of prion diseases, and the minimum lethal dose in hamsters is reported to be less than 2 nM.[4] Thus, discrimination and quantitation of PrP^{Sc} with trace concentrations is important in diagnostics and the monitoring of disease treatment. However, currently used medical practice immunoassays for PrP^{Sc} detection are time- and labor-consuming and require practiced experimental skills.[5−7]

Nanoparticle−organic clusters (NOCs) have attracted wide attention because of their intriguing morphologies and exotic optical properties.[8] NOCs are now promising biofunctional materials for sensing,[9−11] drug delivery,[12] and industrial machinery operation,[13] to name but a few applications. The organic ligands, which connect nanoparticles via coordination bonds, are very important for these NOCs. Our previous research has suggested that PrP^{Sc} molecules assemble into oligomers via intermolecular hydrophobic beta-sheet interactions and hydrogen binding interactions.[14] When PrP is previously modified by particular nanoparticles, specific biosensing systems may be set up. For example, Liang et al.[15] have developed a novel colorimetric method on the basis of the color changes caused by rPrP-induced QD aggregation to detect rPrP. Zhang et al.[16,17] applied gold nanoparticle (AuNP) biosensors for the detection of PrP on the basis of the RLS sensitivity to aggregation and size changes of AuNPs. However, the sensitivity of these RLS and UV−vis methods is restricted by the used spectrometers and their obtained quantitation ranges are narrow.

Surface plasmon resonance (SPR) biosensor technology is a commercialized approach with a higher precision and sensitivity compared with that of traditional immunosorbent assays.[18,19] But due to the low molecular weight (23 kDa) and the trace amount of PrP^{Sc} mixed with the large volume of circulating

Received: September 14, 2017
Accepted: November 22, 2017
Published: November 22, 2017

DOI: 10.1021/acs.analchem.7b03768
Anal. Chem. XXXX, XXX, XXX−XXX

blood, it is highly important for the creation of a novel SPR-based detection assay for PrP^{Sc} detection with ultrasensitivity and high-specificity. Recently, several approaches involving nanotechnology have been reported to enhance the SPR signals.[20] The application of magnetic nanoparticles (MNPs) for SPR signal amplification seems to be the most promising approach because MNPs have magnetic properties that allow for the separation of the target molecules from complicated compounds in the samples to reduce the background interference and further concentrate the analytes.[21,22] Besides, MNPs have a high refractive index and high molecular weight, which effectively increase the SPR signals when MNPs are used as amplification reagents in sandwich SPR methods.[20,23,24] However, all the signals are induced through the binding interactions at the 2-D interfaces between the sensing film and the upper analyte (Figure 1A), and both the signal amplification

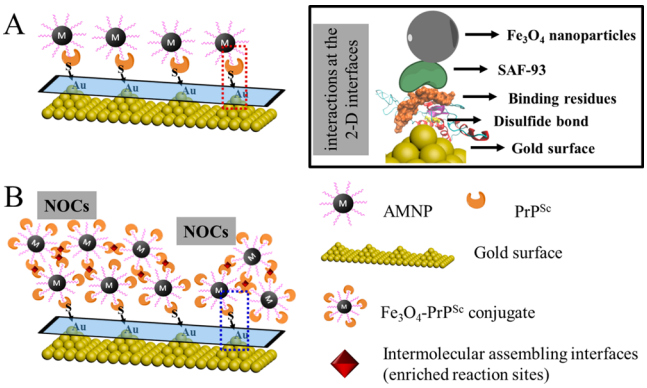

Figure 1. Schematic representations of the traditional sandwich SPR detection format (A) and the facile SPR detection format designed in this work, involving magnetic NOCs (B). Insert: schematic representations of interactions at the 2-D interfaces, which happened in both SPR formats.

level and the maximum quantification concentration are restricted by the amounts of binding sites on the sensing surface.[14] This disadvantage is actually a bottleneck in the routine analyses of PrP^{Sc} in a wide range of concentrations.

As contrast, magnetic NOCs are bioconjugation clusters involving the linking of two or more molecules (PrP^{Sc}) and magnetic nanoparticles (Fe_3O_4) via the intermolecular assembling and specific interactions between bioprobes and analytes, owning the combined properties of its individual components. Besides, when NOCs was introduced to the SPR detection system, the reaction sites contributing the SPR signals are distributed in 3-D space and enriched (Figure 1B). In this work, we constructed a novel SPR detection assay involving magnetic NOCs (Fe_3O_4–PrP^{Sc} clusters) for sensitive PrP^{Sc} detection in a wide range of concentrations. Fe_3O_4 NPs were coated with amino groups through a silanization reaction and then further modified with anti-PrP^{Sc} aptamer (SAF-93) by using glutaraldehyde (GA) as cross-linker. The aptamer-Fe_3O_4 NPs (AMNPs) can specifically capture the free PrP^{Sc} molecules in the sample and quickly concentrate the target by an external magnetic field. By doing this, amorphous clusters involving AMNPs–PrP^{Sc} conjugations were formed, which were confirmed and investigated by high-resolution AFM imaging and molecular simulations. The AMNPs–PrP^{Sc} conjugation clusters (magnetic NOCs) were then injected into the SPR biosensor and detected by the bare gold sensing film through the reactions between the intramolecular disulfide bonds in PrP^{Sc} and the gold atoms.[14] This novel type SPR sensor here (Figure 1A) exhibited excellent analytical performance toward the quantification and quantitation of PrP^{Sc} in a wide concentration range, compared with the traditional 2-D sandwich SPR system (Figure 1B). AFM was used to investigate the morphology of the SPR substrate surface after the detection. To the best of our knowledge, it was the first time that NOCs was combined with the SPR biosensor for the detection of biomolecules. This proposed approach can also be used to detect other analytes with similar assembling behaviors by altering the corresponding aptamer in the AMNPs.

EXPERIMENTAL SECTION

Materials and Reagents. All chemicals were of analytical grade and purchased from Aldrich (Germany). All aqueous solutions were prepared with deionized water. Prion protein was purchased from Calbiochem (Germany, sequence: aa 23–231, theoretical PI/M_w: 9.39/23571.92). The terminal amino functioned anti-PrP^{Sc} aptamer (SAF-93)[25] with 20 thymine bases as the spacer, which has been proven to be of more than 10-fold higher affinity for PrP^{Sc} than for PrP^{C}, were synthesized by Shanghai Sangon Biotechnology Co. in China. ThioPEG was purchased from Prochimia Surfaces in Poland. Cys-protein G (Catalog #:1002–04) was obtained from Shanghai PrimeGene Bio-Tech Co. in China. Newborn calf serum (NBCS) was purchased from ThermoFisher Scientific (Catalog #:1610159). Human serum was purchased from Sigma-Aldrich (St. Louis, MO).

Synthesis and Characterization of Aptamer Modified Fe_3O_4 MNPs. APTES–Fe_3O_4 nanoparticles were prepared by a silanization reaction (Figure S-1A) as described by previous reports.[26,27]

Then, the obtained APTES–Fe_3O_4 (100 μL, 50 mg/mL) was mixed in PBS (900 μL, 100 mM, pH 8.0) containing 0.2% (v/v) glutaraldehyde by ultrasonic dispersion for 20 min in room temperature. After that, amino-modified anti-PrP^{Sc} aptamer (100 μL, 40 μM) was added, followed by 2 h incubation with shaking (150 rpm) in room temperature. This glutaraldehyde cross-linking procedure is in Figure S-1B. To remove the free amino-aptamer and excessive glutaraldehyde, the conjugates were collected by magnetic separation and washed by 100 mM PBS thrice. After that, the conjugates were further ultrafiltrated in a Nanosep 3K Omega filter device (filter size: 30 kDa) until no free aptamer was detected by electrophoresis combined with silver-staining (method details are shown in the next section).

Confirmation of Aptamer-Conjugation on Fe_3O_4 NPs. Aptamer-conjugation on MNPs was confirmed by electrophoresis with 4–20% Mini-PROTEAN TGX Precast Gels (Bio-Rad) in 5× Laemmli Sample buffer. The samples, including marker, free SAF-93, AMNPs, MNPs, and physical mixture of SAF-93 and MNPs, were mixed with loading buffer, heated to 95°C for 10 min, and loaded into the gel. Then the electrophoresis was performed at 180 V for 40 min, and the gels were silver stained with a Focus-Fast silver kit (GBiosciences).

Fabrication of Magnetic NOCs. The formation of AMNPs–PrP^{Sc} conjugation clusters followed the schematic diagram in Figure S-1C. Briefly, 50 μL of AMNPs solution with a certain concentration was first mixed with the samples (1 mL) containing PrP^{Sc} in varied concentrations with other hybrid protein (such as PrP^{C}). Then, the mixtures were incubated at 4 °C for 30 min. During this procedure, PrP^{Sc} was specifically

DOI: 10.1021/acs.analchem.7b03768
Anal. Chem. XXXX, XXX, XXX–XXX

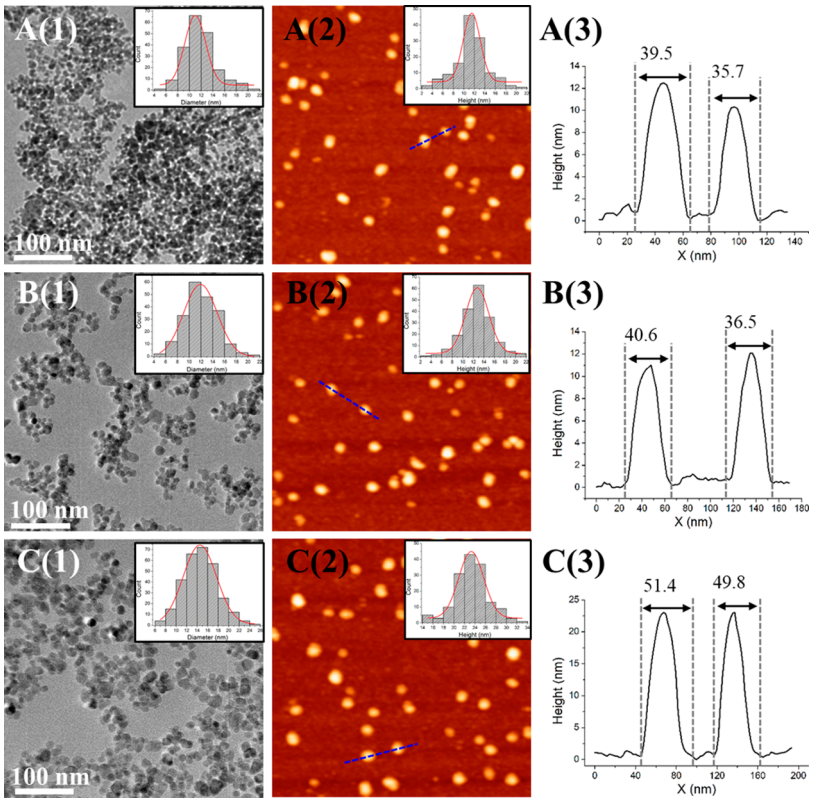

Figure 2. TEM (1) and AFM (2) results of Fe_3O_4 (A), APTES−Fe_3O_4 (B), and AMNPs (C). (3) The corresponding cross section files for the dashed blue lines in their AFM images. Insert: the size distributions of the as-synthesized particles obtained from TEM and AFM, respectively.

captured by AMNPs. After that, the suspensions were collected via a static magnetic field. The concentrated AMNPs−PrP^{Sc} conjugates were redispersed in the PBS buffer via gentle shaking. During this procedure, the magnetic NOCs were formed. To determine the suitable concentration of AMNPs for the capture of the free PrP^{Sc} and for the formation of conjugation clusters, three mixtures of AMNPs with different concentrations and PrP^{Sc} (500 ng/mL) were investigated: A. 1 mg/mL; B. 3 mg/mL; C. 5 mg/mL. The final products were transferred to the liquid cell for AFM investigation.

In situ SPR Measurement. The biosensor system used here is BI-2000 (Biosensing Inc., U.S.A.); the prism is in the Kretschmann configuration, and the gold films (50 nm thick) were also purchased from Biosensing Inc. Prior to the detection, the bare gold film was immersed into the anhydrous acetone overnight to eliminate possible contaminations. After repeatedly washing with water and drying with N_2, the chip was annealed in a hydrogen flame. Then, the sensing film was mounted on a SPR prism with the matching oil. Before the injection of the samples, the chip was rinsed with PBS, and a stable baseline was obtained.

Two kinds of SPR detection formats are investigated in this work: the traditional 2-D sandwich format (Figure 1A) and the novel NOCs enhanced SPR format fabricated in this work (Figures 1B and S-1). For the 2-D sandwich SPR detection, the PrP^{Sc} samples with different concentrations in PBS buffer were successively injected onto the bare gold film. The free PrP^{Sc} molecules were captured on the gold film surface via the hydrogen binding interactions between the intramolecular disulfide bonds and the gold atoms, and relatively low SPR signals were induced.[28] Then, the AMNPs conjugates, which were treated as signal amplification reagents, were injected into the cuvette to enhance the detection signals. The NOC-involved SPR detection was conducted by directly injecting the as-synthesized AMNPs−PrP^{Sc} conjugation clusters (Figure S-1C) into the SPR cuvette, inducing dramatically large SPR signals. All the corresponding SPR signals were obtained in three repeated experiments independently, and the injection rate was set as 15 μL/min.

Detection of PrP^{Sc} in Real Sample. To demonstrate the potential application of this detection system, we detected PrP^{Sc} in human serum by using a standard addition method after mixing 5 mg/mL AMNPs with a series of standard solutions of PrP^{Sc} in nondiluted human serum by vigorous shaking. The mixtures were treated by the procedures as mentioned above, and then, the as-formed NOCs solutions were injected into the SPR cuvette, and a calibration curve was constructed.

Safety Considerations. Prion protein is a potential infective pathogen. All the procedures of manipulating the PrP-containning samples should be performed carefully and should comply with the American Centers for Disease Control (CDC) requirements for biosafety in microbiological and biomedical experiments.[29] All the samples or solutions should be inactivated before removal from the laboratory by adding a sufficient volume of 8 M guanidinium chloride to the final concentration of 6 M. The mixture should be incubated at room temperature for at least 24 h to ensure that the infective molecules are inactivated.[30] The solution of inactivated prions should be transferred to clean fresh containers and removed from the lab.

Characterization. The morphology of the nanoparticle was characterized by transmission electron microscopy (TEM) performed on a FEI Tecnai G^2 20 S-TWIN. The IR spectra were recorded by FT-IR, and each sample together with KBr

DOI: 10.1021/acs.analchem.7b03768
Anal. Chem. XXXX, XXX, XXX−XXX

was pressed to form a tablet. UV−vis spectroscopy was carried out by a UV-3500 spectrophotometer (Shimadzu). Magnetic measurements were carried out using a Lake Shore 7407 VSM (East Changing Technologies, Inc.). AFM was used to investigate the morphologies of the obtained particles, clusters, and the biosensing substrates as in our previous publication.[28]

RESULTS AND DISCUSSION

Characterization of MNPs, APTES-MNPs, and AMNPs. The morphology and structure of the synthesized nanoparticles were examined by both TEM and AFM (Figure 2). It is clearly observed from the TEM results that MNPs, APTES-MNPs, and AMNPs have the same morphology, with an average diameter of 11.00 ± 0.26, 11.92 ± 0.18, and 14.53 ± 0.08 nm. The increased size is attributed to the modification of APTES and SAF-93. The horizontal and vertical dimensions of the nanoparticles are also examined by liquid-phase AFM. Although the measured width of the dots display larger values than the height due to the unavoidable tip broadening effect,[31] the sizes of the nanoparticles can still be observed to increase from ∼35 to ∼50 nm with the modification processes. To be mentioned, the dimensions of AMNPs observed by AFM (23.29 ± 0.56 nm) are dramatically larger than those observed by TEM (14.53 ± 0.08 nm), this may be attributed to the presence of water molecules surrounding the nanoparticles for the liquid AFM imaging..

The modification of the aptamer, SAF-93, to the surface of Fe_3O_4 NPs was confirmed by FT-IR analysis, electrophoresis, and UV−vis spectroscopy. Figure 3A shows the FT-IR spectra

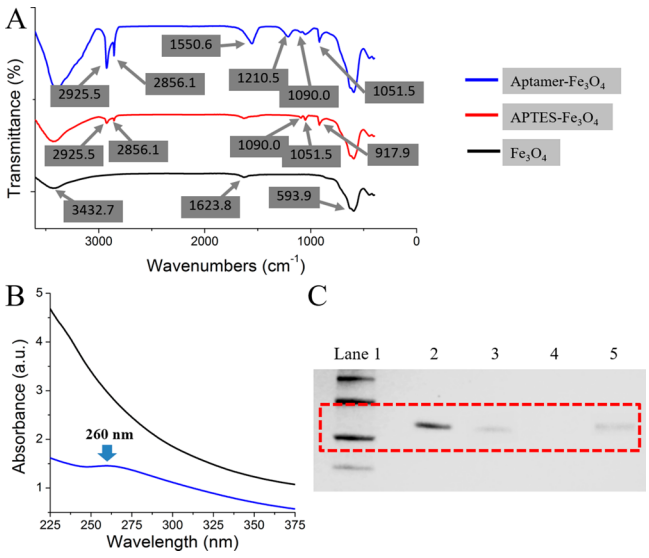

Figure 3. (A) FT-IR results of Fe_3O_4 (black), APTES−Fe_3O_4 (red), and AMNPs (blue). (B) UV−vis spectra of Fe_3O_4 (black) and AMNPs (blue). (C) Silver-stained electrophoresed results of marker (Lane 1), pure SAF-93 (Lane 2), AMNPs (Lane 3), MNPs (Lane 4), and physical mixture of SAF-93 and MNPs (Lane 5).

of the naked Fe_3O_4 (black), APTES−Fe_3O_4 (red), and aptamer−Fe_3O_4 (blue) nanoparticles. For the naked Fe_3O_4, the peak at 593.97 cm^{-1} is because of the Fe−O vibration, and the peak at 3432.7 cm^{-1} is because of the O−H stretching vibration of the water molecules absorbed on the NPs surface, consistent with the previous report.[32] For APTES−Fe_3O_4, compared with the former, intensity enhancement of the peak at 3432.7 cm^{-1} is a result of the O−H stretching and N−H stretching vibrations of APTES. The other characteristic absorption bands of APTES were also observed at 2856.1 and 2925.5 cm^{-1} (C−H stretching vibration), 917.95 cm^{-1} ($-NH_2$ group bending vibration), 1090.0 cm^{-1} (C−N stretching vibration), and 1051.5 cm^{-1} (Si−O stretching vibration).[33] For aptamer−Fe_3O_4, compared with APTES−Fe_3O_4, intensity enhancement of the peaks at 2856.1 and 2925.5 cm^{-1} are attributed to the aptamer. Also, the presence of the DNA-related peak at 1550.6 cm^{-1} and the peak at 1210.5 cm^{-1} are attributed to the stretching vibrations of the PO^{2-} in aptamer, indicating the successful modification of aptamer.[34] It should be mentioned that we are not able to confirm the presence of peaks near 1090 cm^{-1}, implying the C = N cross-linking of aptamer with glutaraldehyde, because the peak overlaps with the C−N stretching vibration of APTES. Figure 3B shows the UV−vis spectra of Fe_3O_4 and aptamer−Fe_3O_4 NPs. There is an obvious broad absorption band at around 260 nm in the spectrum of aptamer−Fe_3O_4 NPs, which is in accordance with the characteristic absorption band of RNA,[35] indicating the successful immobilization of the aptamer on the Fe_3O_4 NPs surface.

The conjugation of SAF-93 to MNPs was also determined by electrophoresis followed by silver staining as shown in Figure 3C. The free aptamer itself (Lane 2) and the free aptamer from the physical mixture (Lane 5) both migrated on the gel and resulted in dark bands. A light band corresponding to the existence of the aptamer is visible for AMNPs purified by ultrafiltration (Lane 3), while MNPs do not show any band on the gel (Lane 4). These data indicated the successful conjugation of SAF-93 to the surface of MNPs.

The essential prerequisite for the concentration and cluster-formation processes is the magnetic properties of AMNPs−PrP^{Sc} conjugates. As shown in Figure S-2, the saturation magnetization of AMNPs−PrP^{Sc} conjugates is 39.07 emu/g, indicating AMNPs have a very fast response to an external magnetic field. As shown in the inset of Figure S-2, after the incubation of AMNPs and PrP^{Sc} at 4 °C for 30 min, the products can be easily collected by an external magnetic field within 20 min.

Molecular Simulation and AFM Investigations of AMNPs−PrP^{Sc} Conjugation Clusters (NOCs) Formation. As in previous studies, the PrP^{Sc} monomer has two hydrophobic β-sheets, with which these monomers can assemble into dimers or trimers by forming a hydrophobic core in aqueous solution.[14,36] These dimers and trimers are proven to assemble via intermolecular hydrogen interactions.[37] The dynamics simulated 3-D structures of the PrP^{Sc} monomer (M), dimer (D), and trimer (T) are shown in Figure S-3A, where the predicted residues involving the intermolecular hydrogen bonds for the formation of conjugation clusters and the specific binding residues toward SAF-93 are labeled in different colors and detailed in Table S-1. The detailed simulation processes are also described in the Supporting Information. From the dynamics simulations, we may see that either the hydrogen binding sites in PrP^{Sc} toward each other, the ones toward SAF-93, or the intramolecular disulfide bond toward the bare gold film are different and in different space orientations. This structural feature promises the formation of the AMNPs−PrP^{Sc} clusters and promises the following binding interactions between the resulting clusters and the bare gold sensing film. The docking simulations of M−D, M−T, and D−T oligomers indicating their predicted morphologies are shown in Figure S-3B, where the binding residues to SAF-93 are active on the

DOI: 10.1021/acs.analchem.7b03768
Anal. Chem. XXXX, XXX, XXX−XXX

outside surface of the 3-D structure. The detailed residues forming the intermolecular hydrogen bonds at the interfaces are listed in Table S-2. All these simulation results indicate that the individual AMNPs−PrP^{Sc} conjugates have possibilities to bind with each other to form conjugation clusters via the intermolecular hydrogen bonds.

The formation of AMNPs−PrP^{Sc} conjugation clusters was confirmed by liquid-phase high-resolution AFM imaging. To determine the suitable concentration of AMNPs for the capture of free PrP^{Sc} and for the formation of AMNPs−PrP^{Sc} conjugate clusters, the as-synthesized products by mixture of AMNPs with different concentrations (1, 3, and 5 mg/mL) and PrP^{Sc} (500 ng/mL) were investigated. After 30 min incubation at 4 °C, the suspensions were collected and transferred to the liquid cell for AFM imaging, respectively. As shown in Figure 4, large and

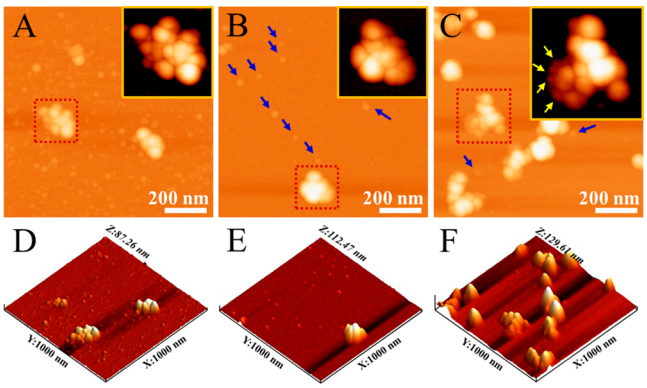

Figure 4. (A−C) AFM images of the conjugation clusters on mica surface obtained by incubating PrP^{Sc} samples with AMNPs in concentrations of 1, 3 and 5 mg/mL, respectively. Insert: Zoom-in AFM images of the squared conjugation clusters in (A−C), respectively. The free PrP^{Sc} molecules are indicated by blue arrows. The supposed captured PrP^{Sc} surrounding the outside of the clusters are indicated by yellow arrows. (D−F) The corresponding 3-D AFM images.

amorphous clusters consisting of obviously bright ball-like dots are observed for all the three mixtures. However, numerous darker and smaller dots coexisting with the clusters are observed on the substrate in Figure 4A,B. Based on their height values, these dots are supposed to be free PrP^{Sc}, indicating that the adsorption of PrP^{Sc} onto AMNPs is saturated, and there were still free PrP^{Sc} not being captured by AMNPs. With the increase of the concentration of AMNPs, we can observe less free PrP^{Sc} are observed on the substrate (pointed by blue arrows in Figure 4B,C) and more clusters appear in the field of AFM (Figure 4C). Based on these results, the AMNPs concentration of 5 mg/mL was chosen for the subsequent assays.

To be mentioned, through the high-resolution zoom-in AFM imaging for these conjugation clusters, we may also observe small dots surrounding the clusters (pointed by yellow arrows in Figure 4C) with similar sizes and morphology to the ones of the observed free PrP^{Sc} in the same visual field (Figure 4A,B). These surrounding dots should be the captured PrP^{Sc} by AMNPs, which are exposed to the external environment ensuring the expected interactions between the conjugation clusters and the gold atoms of the SPR sensing film at the bionano interfaces (Figure 1B).

2-D Sandwich SPR Detection Format for PrP^{Sc}. Figure 5A represents the enhanced SPR signal of the 2-D sandwich

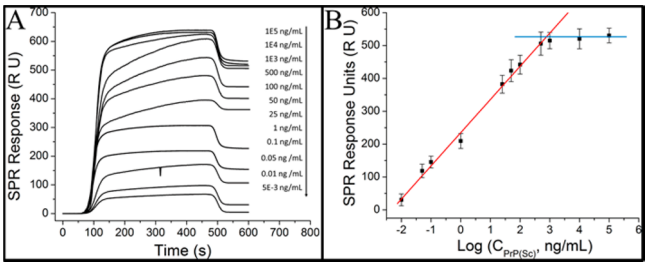

Figure 5. (A) SPR sensorgram and (B) calibration curve of 2-D sandwich SPR detection assay for PrP^{Sc}.

SPR detection format as a function of time. We may observe that the SPR response resulted from the binding of aptamer−MNPs gradually increased with the increased PrP^{Sc} concentration from 0.005 to 100 000 ng/mL. Figure 5B illustrates the variation of the aptamer−MNP-induced signals as a function of PrP^{Sc} concentration. It should be mentioned that the signal of 0.005 ng/mL PrP^{Sc} solution is only 2.66 RU, which is lower than 3σ, indicating that the limit of detection is 0.01 ng/mL (3σ, 30.68 RU). A good linear relationship was obtained between SPR responses and the logarithm of PrP^{Sc} concentrations over a range of 0.01−500 ng/mL. The regression equation was $y = 100.29x + 234.73$ ($R^2 = 0.9887$, x is the logarithm of PrP^{Sc} concentration (log (ng/mL)), and y is the SPR signal (RU)).

Figure S-4 shows the representative AFM images of the morphologies of the SPR substrates after the AMNP amplification detection assay for PrP^{Sc} solutions with concentrations of 0.1, 1, and 500 ng/mL, respectively. It is obvious that the higher concentration induced a higher degree of surface immobilized AMNPs. When the PrP^{Sc} concentration is 1 ng/mL, some naked regions without AMNPs were observed after the successive injections of PrP^{Sc} and AMNPs solutions via AFM and highlighted in Figure S-4B. When the concentration of PrP^{Sc} increased from 1 to 500 ng/mL, the conjugates were observed to entirely cover the sensing substrate (Figure S-4C). And there would be hardly more bindings of the magnetic conjugates onto the sensing substrate by further increasing the PrP^{Sc} concentration. This is the reason why the SPR-enhanced signal increased slightly when the concentration of PrP^{Sc} is higher than 500 ng/mL, as in Figure 5. This confirmed the bottleneck of the 2-D sandwich format mentioned above.

Before the injection of the signal amplification reagents, the previously captured PrP^{Sc} molecules, the magnetic conjugates, could be observed by high-resolution AFM imaging. Figure S-4G is the cross section profile for the yellow dashed line in Figure S-4A. As shown in Figure S-4G, the heights of the bright dots (~20 nm) are consistent to the measured height values of AMNPs in Figure 2, indicating the modification of AMNPs on the substrate. Besides, lower signals at around 1 nm (insert in Figure S-4G) are observed, which are consistent to our reported height values of PrP^{Sc} units (M, D, and T).[38] And from the zoom-in image (Figure S-4H) of the substrate, we are also able to visualize smaller dots with similar height values at around 1 nm (Figure S-4I). All these results indicate that these observed dot-like particles were the captured PrP^{Sc} molecules by sensing film.

Magnetic-NOC-Enhanced SPR Sensing for the Detection of PrP^{Sc}. As we discussed above, the AMNPs can capture the free PrP^{Sc} molecules in the solution via the specific

DOI: 10.1021/acs.analchem.7b03768
Anal. Chem. XXXX, XXX, XXX−XXX

interaction between the modified aptamer (SAF-93) and PrP^{Sc}. The PrP^{Sc}–AMNPs conjugations can then form conjugate clusters via the intermolecular hydrogen binding interactions among these captured PrP^{Sc} (Figures S-3B and 4). To evaluate the performance of the PrP^{Sc}–AMNPs conjugation-cluster-enhanced SPR sensing, PrP^{Sc} at various concentrations (1×10^{-4}–1×10^{5} ng/mL) was treated by 5 mg/mL AMNPs through a series of procedures as shown in Figure S-1C. Then the magnetic NOCs solutions were injected into the SPR cell, respectively. The in situ SPR curves and the calibration curves are shown in Figure 6. As seen in Figure 6A, the SPR response

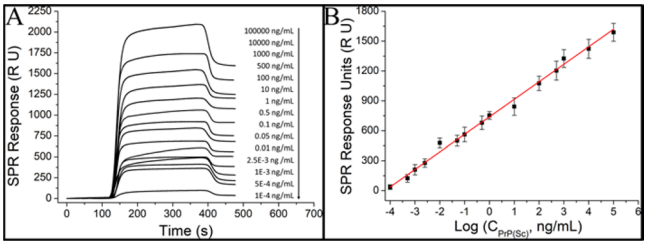

Figure 6. (A) SPR sensorgram and (B) calibration curve of NOC-involved SPR detection assay for PrP^{Sc}.

resulting from the capture of NOCs onto the sensing film gradually increased with the increasing initial PrP^{Sc} concentration. Figure 6B illustrates the variation of the concentration-cluster-induced signal as a function of PrP^{Sc} concentration. A good linear relationship is obtained between SPR responses and the logarithm of PrP^{Sc} concentrations over a wide concentration range from 1×10^{-4} to 1×10^{5} ng/mL. The regression equation is $y = 175.80x + 740.10$.

The SPR responses of the direct, AGO (aptamer-modified graphene oxide[28])-enhanced, 2-D sandwich (this work) and the NOC-involved SPR detection format (this work) are collected in Figure S-5 as a function of initial PrP^{Sc} concentration. As seen in Figure S-5, the NOC-involved SPR detection format yields the highest enhancement degree of the signals among these four detection formats. The magnetic NOCs permit a 215-fold increase of the direct SPR signal, while the AGO permits a 152-fold increase, and the AMNPs permit only a 65-fold increase. Based on this dramatic signal enhancement capacity, the limit of detection (LOD) of the NOC-involved SPR format is as low as 0.0001 ng/mL, which is 10 and 100 times lower than that of AGO and the 2-D sandwich format, respectively. Also, the quantitative concentration of the NOC-involved SPR detection format is up to 100 000 ng/mL, while the AGO and 2-D sandwich format is only 0.001 and 1 ng/mL respectively. The highest sensitivity and the largest quantitative detection range of the NOC-involved format are not only due to the high refractive index and high molecular weight of AMNPs but also are independent of the number of the binding sites on the gold film surface and the lack of an effect from the steric hindrance compared to that of the other two formats. As shown in Figure 7, it is obvious from the AFM imaging of the surface morphology of NOC-modified SPR sensing substrate that the SPR gold surfaces are entirely covered by the NOCs for all these three concentrations, which is different from the 2-D sandwich format. In addition, their corresponding height values are much larger than those of the 2-D sandwich format, indicating larger degrees of depositions of amplification reagents. This should be the main explanation for the excellent signal amplification effect of magnetic NOC-involved SPR

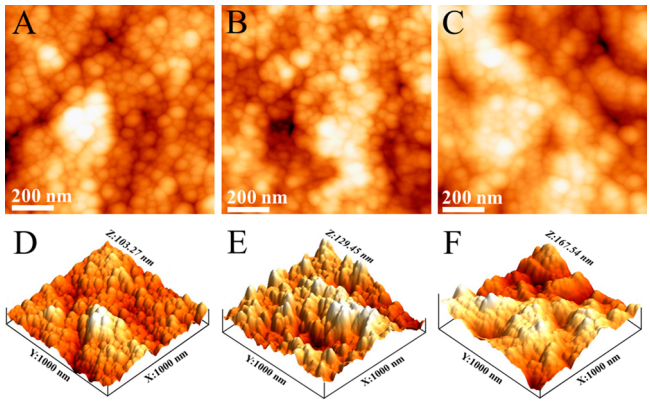

Figure 7. (A–C) AFM images of SPR gold surfaces after the NOC-involved amplification detection assay for PrP^{Sc} solutions with concentrations of 1, 500, and 10 000 ng/mL, respectively. (D–F) The corresponding 3-D AFM iamges.

detection assay. However, considering the submicrometer size of NOCs and the fact that SPR only measures the changes in the amount of material within about 200 nm upon the sensing surface,[38] the exact maximum quantitative detection limit of NOC-involved format constructed here is dependent on the real case, such as the average size of the formed NOCs and the actual size of the injection catheter of the commercial SPR instrument.

Selectivity and Specificity. To evaluate the selectivity and specificity of the amplification detection format with magnetic NOCs, PrP^{Sc} (10 ng/mL) in both PBS buffer and NBCS, three different reagents (MPA, thioPEG, and Cys-protein G, 10 ng/mL), which all have sulfhydryl groups and can assemble on the gold surface,[39–41] PrP^{C} (10 ng/mL), and the mixture of PrP^{Sc} (10 ng/mL) with each of the four different regents (10 ng/mL) were measured using the amplification detection format, respectively. The results are shown in Figure 8, from which it

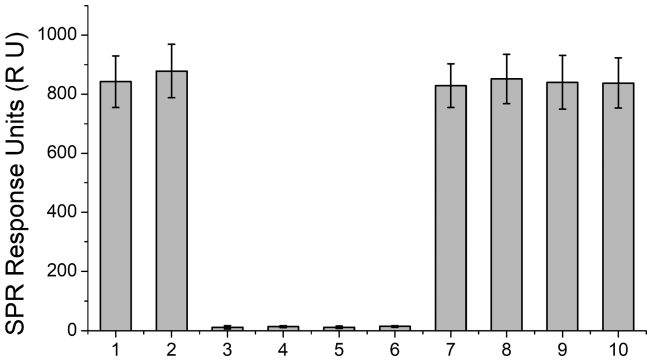

Figure 8. Specific analysis of magnetic NOC-involved SPR amplification detection. 1: PrP^{Sc} (10 ng/mL) in PBS buffer; 2: PrP^{Sc} (10 ng/mL) in NBCS; 3–6: MPA, thioPEG, Cys-protein G, and PrPC (10 ng/mL each) in PBS buffer, respectively; 7–10: mixture of PrP^{Sc} (10 ng/mL) and each of the four different regents (10 ng/mL) in PBS buffer.

can be observed that PrP^{Sc} has an average response of ~850 RU, which was much greater than that of the other four regents (~15 RU). In addition, similar SPR responses were obtained for PrP^{Sc} in four mixed samples, indicating that these four regents have no effect to the SPR detection response of the PrP^{Sc} in the mixture sample. All the results confirm that the

DOI: 10.1021/acs.analchem.7b03768
Anal. Chem. XXXX, XXX, XXX–XXX

NOC-involved SPR approach has a sufficient specificity for PrP^{Sc} detection.

Detection of PrP^{Sc} in Human Serum. A calibration curve was obtained after detecting PrP^{Sc} in human serum using the NOC-involving SPR detection system constructed in this work (Figure S-6). The linear regression equation was $y = 149.74x + 764.70$ ($R^2 = 0.9715$, x is the logarithm of PrP^{Sc} concentration (log (ng/mL)), and y is the SPR signal (RU)). The RSD was 2.37% ($n = 5$) for 0.01 ng/mL PrP^{Sc}. The corresponding recovery is 105%. This good linearity and recovery showed that the detection assay constructed here could be applied in the detection of PrP^{Sc} in a real sample.

CONCLUSIONS

We constructed a novel SPR detection assay utilizing PrP^{Sc} conjugating magnetic nanoparticle clusters as signal amplification reagents for the ultrasensitive detection of PrP^{Sc}. Magnetic NOCs were obtained after the incubation of AMNPs and PrP^{Sc} and the subsequent concentration processes in an external magnetic field. The conjugation clusters were further injected into the SPR cuvette and captured onto the gold sensing film via an Au−S bonding interaction, inducing intense SPR responses. Meanwhile, a traditional 2-D sandwich SPR detection format simply using gold/PrP^{Sc}/AMNPs amplification mode was conducted for detection of PrP^{Sc} as a comparison. The results reveal that NOC-involved SPR format permits a 215-fold increase of the direct SPR signal, while the 2-D sandwich format permitted only a 65-fold increase. Moreover, a lower detection limit (1×10^{-4} ng/mL) and a wider quantitation range (1×10^{-4}−1×10^{5} ng/mL) are demonstrated. The formation of the conjugation clusters were investigated by high-resolution AFM imaging and molecular simulations. This conjugation-cluster-induced signal amplification strategy has great potential for detection of small analytes with similar structural characteristics in trace level concentration with high selectivity and sensitivity by altering the corresponding aptamer labeled to magnetic particles.

ASSOCIATED CONTENT

Supporting Information

The Supporting Information is available free of charge on the ACS Publications website at DOI: 10.1021/acs.analchem.7b03768.

Schematic representations, VSM results, dynamics simulations, AFM imaging, collection of the detection results of various SPR formats, calculated curve of SPR detection in human serum (PDF)

AUTHOR INFORMATION

Corresponding Authors

*E-mail: zc-lou2015@njfu.edu.cn; Tel: +86-18251978955 (Z.L.)

*E-mail: guning@seu.edu.cn (N.G.)

ORCID

Zhichao Lou: 0000-0002-0819-9347

Ning Gu: 0000-0003-0047-337X

Notes

The authors declare no competing financial interest.

ACKNOWLEDGMENTS

This work was supported by the National Natural Science Foundation of China (No. 61601227), the Nature Science Foundation of Jiangsu Province (BK20160939), the Natural Science Foundation of the Jiangsu Higher Education Institutions of China (16KJB180010), and the Qing Lan Project and Priority Academic Program Development of Jiangsu Higher Education Institutions (PAPD).

REFERENCES

(1) Harris, D. A. *Clin. Microbiol. Rev.* **1999**, *12*, 429−444.

(2) Shyng, S. L.; Huber, M. T.; Harris, D. A. *J. Biol. Chem.* **1993**, *268*, 15922−15928.

(3) Biasini, E.; Turnbaugh, J. A.; Unterberger, U.; Harris, D. A. *Trends Neurosci.* **2012**, *35*, 92−103.

(4) MacGregor, I. R.; Drummond, O. *Vox Sang.* **2001**, *81*, 236−240.

(5) Chen, B.; Morales, R.; Barria, M. A.; Soto, C. *Nat. Methods* **2010**, *7*, 519−520.

(6) Englund, H.; Sehlin, D.; Johansson, A.-S.; Nilsson, L. N. G.; Gellerfors, P.; Paulie, S.; Lannfelt, L.; Pettersson, F. E. *J. Neurochem.* **2007**, *103*, 334−345.

(7) Reuter, T.; Gilroyed, B. H.; Alexander, T. W.; Mitchell, G.; Balachandran, A.; Czub, S.; McAllister, T. A. *J. Microbiol. Methods* **2009**, *78*, 307−311.

(8) Colvin, V. L.; Kulinowski, K. M. *Proc. Natl. Acad. Sci. U. S. A.* **2007**, *104*, 8679−8680.

(9) Ding, X.; Zeng, D.; Xie, C. *Sens. Actuators, B* **2010**, *149*, 336−344.

(10) Huang, R.-W.; Wei, Y.-S.; Dong, X.-Y.; Wu, X.-H.; Du, C.-X.; Zang, S.-Q.; Mak, T. C. W. *Nat. Chem.* **2017**, *9*, 689−697.

(11) Lin, L.; Hu, Y.; Zhang, L.; Huang, Y.; Zhao, S. *Biosens. Bioelectron.* **2017**, *94*, 523−529.

(12) Cho, M. H.; Kim, S.; Lee, J.-H.; Shin, T.-H.; Yoo, D.; Cheon, J. *Nano Lett.* **2016**, *16*, 7455−7460.

(13) Sun, J.; Yan, Y. *Chem. Eng. J.* **2017**, *323*, 381−395.

(14) Lou, Z.; Wang, B.; Guo, C.; Wang, K.; Zhang, H.; Xu, B. *Colloids Surf., B* **2015**, *135*, 371−378.

(15) Liang, L.; Long, Y.; Zhang, H.; Wang, Q.; Huang, X.; Zhu, R.; Teng, P.; Wang, X.; Zheng, H. *Biosens. Bioelectron.* **2013**, *50*, 14−18.

(16) Zhang, H.-J.; Lu, Y.-H.; Long, Y.-J.; Wang, Q.-L.; Huang, X.-X.; Zhu, R.; Wang, X.-L.; Liang, L.-P.; Teng, P.; Zheng, H.-Z. *Anal. Methods* **2014**, *6*, 2982−2987.

(17) Zhang, H.-J.; Zheng, H.-Z.; Long, Y.-J.; Xiao, G.-F.; Zhang, L.-Y.; Wang, Q.-L.; Gao, M.; Bai, W.-J. *Talanta* **2012**, *89*, 401−406.

(18) Hoa, X. D.; Kirk, A. G.; Tabrizian, M. *Biosens. Bioelectron.* **2007**, *23*, 151−160.

(19) Situ, C.; Mooney, M. H.; Elliott, C. T.; Buijs, J. *TrAC, Trends Anal. Chem.* **2010**, *29*, 1305−1315.

(20) Zeng, S.; Baillargeat, D.; Ho, H.-P.; Yong, K.-T. *Chem. Soc. Rev.* **2014**, *43*, 3426−3452.

(21) Kim, J. I.; Wang, C. H.; Kuizon, S.; Xu, J. L.; Barengolts, D.; Gray, P. C.; Rubenstein, R. *J. Neuroimmunol.* **2005**, *158*, 112−119.

(22) Skaat, H.; Sorci, M.; Belfort, G.; Margel, S. *J. Biomed. Mater. Res., Part A* **2009**, *91A*, 342−351.

(23) Liang, R.-P.; Yao, G.-H.; Fan, L.-X.; Qiu, J.-D. *Anal. Chim. Acta* **2012**, *737*, 22−28.

(24) Wang, J.; Zhu, Z.; Munir, A.; Zhou, H. S. *Talanta* **2011**, *84*, 783−788.

(25) Rhie, A.; Kirby, L.; Sayer, N.; Wellesley, R.; Disterer, P.; Sylvester, I.; Gill, A.; Hope, J.; James, W.; Tahiri-Alaoui, A. *J. Biol. Chem.* **2003**, *278*, 39697−39705.

(26) Hong, R.-Y.; Li, J.-H.; Zhang, S.-Z.; Li, H.-Z.; Zheng, Y.; Ding, J.; Wei, D.-G. *Appl. Surf. Sci.* **2009**, *255*, 3485−3492.

(27) Yamaura, M.; Camilo, R. L.; Sampaio, L. C.; Macêdo, M. A.; Nakamura, M.; Toma, H. E. *J. Magn. Magn. Mater.* **2004**, *279*, 210−217.

(28) Lou, Z.; Wan, J.; Zhang, X.; Zhang, H.; Zhou, X.; Cheng, S.; Gu, N. *Colloids Surf., B* **2017**, *157*, 31−39.

DOI: 10.1021/acs.analchem.7b03768
Anal. Chem. XXXX, XXX, XXX−XXX

(29) Centers for Disease Control and Prevention (U.S.); National Institute of Health (U.S.). *Biosafety in Microbioloical and Biomedical Laboratories*, 5th ed.; U.S. Dept. of Health and Human Services: Washington, D. C., 2009.
(30) Prusiner, S. B.; Groth, D.; Serban, A.; Stahl, N.; Gabizon, R. *Proc. Natl. Acad. Sci. U. S. A.* **1993**, *90*, 2793−2797.
(31) Radmacher, M.; Fritz, M.; Hansma, H. G.; Hansma, P. K. *Science* **1994**, *265*, 1577−1579.
(32) Lou, Z.; Zhou, Z.; Zhang, W.; Zhang, X.; Hu, X.; Liu, P.; Zhang, H. *J. Taiwan Inst. Chem. Eng.* **2015**, *49*, 199−205.
(33) Ma, M.; Zhang, Y.; Yu, W.; Shen, H. Y.; Zhang, H. Q.; Gu, N. *Colloids Surf., A* **2003**, *212*, 219−226.
(34) Wang, J.; Munir, A.; Zhu, Z.; Zhou, H. S. *Anal. Chem.* **2010**, *82* (16), 6782−6789.
(35) Bürger, A.; Wagner, C.; Viedt, C.; Reis, B.; Hug, F.; Hänsch, G. M. *Kidney Int.* **1998**, *54*, 407−415.
(36) Pan, K. M.; Baldwin, M.; Nguyen, J.; Gasset, M.; Serban, A.; Groth, D.; Mehlhorn, I.; Huang, Z.; Fletterick, R. J.; Cohen, F. E. *Proc. Natl. Acad. Sci. U. S. A.* **1993**, *90*, 10962−10966.
(37) Stoehr, J.; Weinmann, N.; Wille, H.; Kaimann, T.; Nagel-Steger, L.; Birkmann, E.; Panza, G.; Prusiner, S. B.; Eigen, M.; Riesner, D. *Proc. Natl. Acad. Sci. U. S. A.* **2008**, *105* (7), 2409−2414.
(38) George, P. *Encyclopedia of Immunology* **1998**, No. 4, 2247−2250.
(39) Dong, S.; Li, J. *Bioelectrochem. Bioenerg.* **1997**, *42* (1), 7−13.
(40) Le Brun, A. P.; Holt, S. A.; Shah, D. S. H.; Majkrzak, C. F.; Lakey, J. H. *Biomaterials* **2011**, *32* (12), 3303−3311.
(41) Lee, J. M.; Park, H. K.; Jung, Y.; Kim, J. K.; Jung, S. O.; Chung, B. H. *Anal. Chem.* **2007**, *79* (7), 2680−2687.

DOI: 10.1021/acs.analchem.7b03768
Anal. Chem. XXXX, XXX, XXX−XXX